Comparison of SSM/I and AMSR-E Sea Ice Concentrations With ASPeCt Ship Observations Around Antarctica

Alexander Beitsch, Stefan Kern, and Lars Kaleschke

***Abstract*—We compare passive microwave (PM)-derived sea ice concentrations (SIC) with more than 21 600 ship-based observations (OBS) of SIC acquired around Antarctica. PM SIC are derived from SSM/I-SSMIS and AMSR-E measurements in 1991–2009 and 2002–2010, respectively, with the ARTIST Sea Ice (ASI), Comiso Bootstrap (BST), NASA-Team (NT), enhanced NASA-Team (NT2), and EUMETSAT OSI-SAF (OSI) algorithm. We compare correlation coefficients (CC), RMSDs, and biases, separately for SSM/I-SSMIS data for algorithms ASI, BST, OSI, and NT, and for AMSR-E data for algorithms ASI, BST, and NT2. With OBS SIC and PM SIC being on fundamentally different spatiotemporal scales, we develop a new colocation approach using daily-average along-ship-track SIC values. CC between OBS SIC and PM SIC agree within their uncertainty for all algorithms and sensors. Year-round CC values are around 0.85 (AMSR-E) and 0.82 (SSM/I); CC values are similar during summer, but drop significantly during winter. Year-round RMSD values range from 13% (BST and OSI) to 17% (NT) for SSM/I and from 12% (BST) to 16% (NT2) for AMSR-E. RMSD values are similar during summer, but decrease for winter (BST: 8% for AMSR-E, 10% for SSM/I). For AMSR-E, biases are below 0.5% for BST and ASI, but between 5% (winter) and 9% (summer) for NT2. For SSM/I, biases are smaller during summer, −0.7% for BST to −7.8% for NT, than winter, −3.6% for BST to −13.9% for NT. Overall, best agreement between OBS and PM SIC is found for BST.**

***Index Terms*—Antarctic, Antarctic sea ice processes and climate (ASPeCt), passive microwave (PM) remote sensing, sea ice concentration (SIC), ship-based observations (OBS).**

I. Introduction

THE Antarctic continent and surrounding sea-ice-covered regions are vast and remote. Precise knowledge about the sea ice extent and concentration is needed for many applications in geoscientific research, e.g., for modeling the formation of deep water masses [1] and for providing realistic boundary conditions when modeling quantities that are dependent on sea surface and ice conditions [2], [3]. The only tool to receive weather- and daylight-independent daily coverage of the current large-scale ice situation is satellite microwave radiometry. Measured brightness temperatures are input to retrieval algorithms that detect sea ice concentration (SIC), which, among other differences, use distinct combinations of frequencies and polarization to retrieve SIC. Validation of retrieved SIC is possible by comparing with ground truth data, for example, from vessels navigating through the sea ice cover. The longest ship-based observation (OBS) data set of the Antarctic sea ice cover is available through the Antarctic Sea Ice Processes and Climate (ASPeCt) program, which collects observations that have been carried out following the ASPeCt standards, that are also known as the ASPeCt protocol. Several studies have been using single or sequences of cruises that contribute to the ASPeCt data as a ground truth data source for comparison with satellite passive microwave (PM) SIC products based on Special Sensor Microwave/Imager (SSM/I), Special Sensor Microwave Imager/Sounder (SSMIS) and Advanced Microwave Scanning Radiometer for the Earth Observing System (AMSR-E) measurements [4]–[6]. However, to our knowledge, there has not been a study using all available ASPeCt data extended by OBS from cruises in recent years and comparing them with the most used SIC retrieval algorithms. In this paper, we want to assess the quality and performance of the most used SIC retrieval algorithms by comparing with an extended ASPeCt data set around Antarctica. Moreover, we want to infer if there are significant differences among the tested algorithms or if there exists one algorithm that we can recommend as the most reliable algorithm providing data of daily PM-derived SIC.

Prior to this paper, Worby and Comiso [4] investigated the sea ice edge derived from SIC data with two different algorithms, namely, the enhanced NASA Team (NT2) and Bootstrap (BST), based on SSM/I measurements and ASPeCt data in the years 1989–2000. Regarding geographical latitude, they find an accurate detection of the ice edge between March and October with maximum mean differences of 0.11°. SIC that are derived using BST give the best results. Correlations are reduced during the melt season (November–February), when the sea ice and its snow cover become wet and flooded, so that surface signatures appear as a mixture of ice and open water to microwave sensors. Tekeli *et al.* [7] examined data from field cruises in West Antarctica, comparing snow and ice properties derived by Envisat Advanced Synthetic Aperture Radar

Manuscript received October 3, 2013; revised March 24, 2014 and June 11, 2014; accepted July 14, 2014. This work was supported by the Bundesministerium für Wirtschaft und Technologie (Federal Ministry of Economics and Technology) through the project "Ice-Route-Optimization-2" under Grant U-4-6-03-BMW-11-02 in the framework of the program "Shipping and ocean engineering for the 21st century" and by the Deutsche Forschungsgemeinschaft (German Research Foundation) through the Cluster of Excellence (CliSAP, EXC 117). The work of S. Kern was supported by the International Space Science Institute (ISSI), Bern, Switzerland, under Project #245: Heil, P. and S. Kern, "Towards an Integrated Retrieval of Antarctic Sea Ice Volume".

A. Beitsch was with the Institute of Oceanography, University of Hamburg, 20146 Hamburg, Germany. He is now with the Max Planck Institute for Meteorology, 20146 Hamburg, Germany (e-mail: alexander.beitsch@zmaw.de).

S. Kern is with KlimaCampus/CliSAP, University of Hamburg, 20144 Hamburg, Germany.

L. Kaleschke is with the Institute of Oceanography, University of Hamburg, 20146 Hamburg, Germany.

Color versions of one or more of the figures in this paper are available online at http://ieeexplore.ieee.org.

Digital Object Identifier 10.1109/TGRS.2014.2351497

(ASAR), AMSR-E measurements and ASPeCt observations. In particular, during the melt season, radar properties of thick first- and multiyear ice are altered and a correct interpretation of the observed radar backscatter values, and their variation over time becomes difficult to make. Kern [8] compared about 850 OBS taken during several cruises in 1994–1998 with BST, the PELICON algorithm [9], and the SEA LION algorithm [10], [11]. All algorithms underestimate OBS SIC by 5% to 17% and show correlations below 0.6. Knuth and Ackley [5] compared SSM/I-based NT SIC and BST SIC with OBS SIC from three cruises and one helicopter-based data set during 1999–2004. While from December to mid-February, PM SIC over- and underestimate OBS SIC to an equal amount, PM SIC provide better estimates of OBS SIC from mid-February to April, when air temperatures drop. Correlations tend to be higher for fall data. Estimates of NT's maximum error ($\sim$15%) exceed those of BST ($\sim$10%) and the $\sim$10% observation error for OBS—Weissling *et al.* [12] confirmed the average accuracy of ASPeCt SIC observations to be 10% or better. In accordance with Nihashi *et al.* [13], Knuth and Ackley [5] found floe size and resolution as the most contributing factors of PM SIC's underestimation in a medium-range SIC regime ($< 70\%$). Ozsoy-Cicek *et al.* [6] examined AMSR-E-based SIC of NT2 and BST for their accuracy in detecting the SIC, the sea ice extent, and the location of the sea ice edge and compare them with ASPeCt OBS. A good correlation was found inside the ice pack, but the correlation reduced in the Marginal Ice Zone (MIZ). Both sets of SIC, NT2 and BST, tend to underestimate low ice concentrations and show the location of the ice edge further south than ASPeCt OBS. This becomes particularly apparent during melting conditions. Ozsoy-Cicek *et al.* [14] made similar investigations for other cruises finding a low ice concentration bias with AMSR-E-based sea ice extents showing the tendency to underestimate U.S. National Ice Center ice edges.

Despite this number of studies using single cruise observational data sets or a limited number of years from the ASPeCt data, there has not been a comparison of the full record of ASPeCt ship-based SIC observations with SSM/I-SSMIS and AMSR-E SIC. Here, we present a comparison of OBS SIC from extended ASPeCt data, which we regard as ground truth, with different PM SIC data. We append additional OBS SIC to the freely available ASPeCt data set (http://aspect.antarctica.gov.au) from other cruises in 2006–2011 where SIC have been observed according to the ASPeCt protocol [15]. For the comparison, we use different PM SIC to compare with the extended ASPeCt data. Four of the PM SIC data sets are based on SSM/I-SSMIS measurements and three data sets are based on AMSR-E measurements. We do a third comparison, in which we compare two algorithms, namely, BST and ASI, which provide SIC that are based on measurements of both sensors, SSM/I-SSMIS, and AMSR-E. This henceforth called sensor comparison emphasizes differences due to the different spatial resolutions of the sensors. We assess the performance of PM SIC by calculating correlation coefficients (CC), root-mean-square deviations (RMSD), and bias with respect to OBS SIC. Eventually, we are able to rank the SIC retrieval algorithms used for comparison in this paper.

This paper proceeds in the following way: Section II gives details about the sensors and the PM SIC data used, as well as an explanation of the method we apply to compare those data sets with OBS. Section III describes the results for the different comparisons, namely, the SSM/I-SSMIS-based comparison, the AMSR-E-based comparison, and the sensor comparison. In Section IV, we discuss our results and we end with our conclusions in Section V.

II. Data and Methods

A. Reference Ground-Truth Data Set: The Extended ASPeCt Data Set

The ASPeCt data archive contains data from 81 voyages and 1663 aircraft-based observations for the period 1980–2005 [16]. The data contain each individual observation, including characteristics of different ice types and snow cover. We use the total SIC, which, among other quantities, is estimated visually from the ship's bridge typically every hour, while the ship is within an ice cover. A single ship observation accounts for an elliptically shaped area with about 1 km semiminor axis. The ellipse's semimajor axis is aligned along the ship track. Ideally, the observation area should be a disk of 1 km radius. However, due to the ship's movement and the average duration of each observation of 5 to 10 min, this disk is distorted to an ellipse. With reduced visibility due to fog, clouds, or precipitation, the area of observation can be even further reduced. Each individual OBS SIC is compared with the value from a PM SIC grid cell colocated to that location as will be described later.

We extend the ASPeCt data set with sea ice observations from cruises in 2006–2011. The ice observations on these cruises have been carried out according to the ASPeCt protocol. The appended data were collected on the following cruises:

- WWOS (September–October 2006; S. Willmes, pers. comm.; [17]);
- SIMBA and SIPEX (September–October 2007; B. Ozsoy-Cicek, pers. comm.; [14]);
- ODEN and PALMER (December 2007–January 2008, December 2008–January 2009, January–February 2009; A. H. Tekeli, pers. comm.; [7]);
- ICEBELL (November–December 2010; S. Ackley, pers. comm.);
- ODEN (December 2010–January 2011; S. Ackley, pers. comm.)

Limitations exist for the accuracy of the ASPeCt observations, i.e., OBS SIC. Total SIC is estimated to the nearest 10%, which can give a rounding error of up to 5%. A human ice observation is subjective and prone to contain errors that may vary between observers and are difficult to quantify. However, tests with different observers have shown that simultaneous observations of total SIC rarely differ by more than 10% [4]. Due to the duration of a single ice observation, the SIC estimate can represent an average of the real ice situation [12]. In particular, in the MIZ, SIC changes can be abrupt over short time scales with alternating bands of open water and consolidated ice. Depending on the weather situation, visibility can be low, reducing the validity of the observed SIC value. To ensure as much consistency as possible, the ASPeCt data have been taken through quality control processes [15]. The analysis carried out by Weissling *et al.* [12] confirms that the average accuracy of ASPeCt SIC observations is 10% or better.

TABLE I
FOOTPRINT SIZES (IN km × km) OF THE DIFFERENT CHANNELS OF SSM/I [23], SSMIS [24], AND AMSR-E [21]

Frequency (GHz)	19.35 (SSM/I)	22.235 (SSM/I)	37.0 (SSM/I)	85.5 (SSM/I)
	19.35 (SSMIS)	22.235 (SSMIS)	37.0 (SSMIS)	91.655 (SSMIS)
	18.7 (AMSR-E)	23.8 (AMSR-E)	36.5 (AMSR-E)	89.0 (AMSR-E)
SSM/I	43x69	40x60	28x37	13x15
SSMIS	45x74	45x74	28x45	13x15
AMSR-E	16x27	18x32	8x14	4x6

TABLE II
OVERVIEW OF THE SIC ALGORITHMS; "V" AND "H" REFER TO VERTICAL AND HORIZONTAL POLARIZATION, RESPECTIVELY

Algorithm	**Acronym**	**Channels used for retrieval**	**References**
ARTIST Sea Ice	ASI	85/91/89V, 85/91/89H	Svendsen *et al.* [37], Kaleschke *et al.* [33], Spreen *et al.* [22]
Bootstrap Comiso	BST	19V, 37V	Comiso *et al.* [38], and references therein
Bristol	BRI	19V, 19H, 37V, 37H	Smith [32]
EUMETSAT OSI-SAF	OSI	19V, 19H, 37V, 37H	EUMETSAT [30], Eastwood *et al.* [31], Tonboe and Nielsen [39]
NASA-Team	NT	19V, 19H, 37V	Comiso *et al.* [38], and references therein
NASA-Team-2	NT2	19V, 19H, 37V, 37H, 85/91/89V, 85/91/89H	Markus and Cavalieri [27]

B. SIC From Satellite Data

The SSM/I instrument was launched onboard the Defense Meteorological Satellite Program (DMSP) satellites. These satellites circuit the Earth in a sun-synchronous, near-circular, polar orbit. During one day, a complete coverage of the polar regions is achieved. The instrument is a multichannel PM radiometer scanning the ground scene at constant angle of about 53° incidence angle [18]. With the launch of DMSP F-16, SSM/I has been replaced by its successor, i.e., the SSMIS instrument. SSMIS augments SSM/I's imaging channels by several atmospheric sounding channels, but still holds SSM/I's capabilities in recording brightness temperatures (Tb) with imaging channels that are relevant for SIC retrievals, namely, the 19 GHz, the 22 GHz, the 37 GHz, and the 85 GHz imaging channels. The 85 GHz data provide higher spatial resolution and thus a finer grid resolution in contrast to the low-frequency channels usually used for SIC retrievals; the area of one 85 GHz grid cell is just one-fourth of the grid cell area of the low-frequency channels. 85 GHz data became only usable with DMSP F-11 in late 1991; for SSM/I on DMSP-F8 and DMSP-F10, the 85 GHz channels were too noisy at time and could not be used [19]. For coherency, data from SSM/I and SSMIS have been intercalibrated [20].

The AMSR-E instrument was launched aboard the Aqua satellite [21]. Like the DMSP satellites, Aqua is on a sun-synchronous, near-circular, and polar orbit. The AMSR-E instrument scans at similar frequencies and at a similar incidence angle such as the SSM/I and SSMIS instruments but has an improved spatial resolution in comparison to SSM/I and SSMIS instruments (see Table I). For instance, the resolution of the AMSR-E 89 GHz channels is about three times finer than for the SSM/I 85 GHz channels, which reduces the 85-/89-GHz footprint area by a factor of 8 [22].

From this point onward, we refer to the combined SIC databased on SSM/I and SSMIS measurements when we mention SSM/I.

C. SIC Retrieval Algorithms

The SIC data used in the SSM/I comparison are based on the ASI, the NASA Team (NT), the BST, and EUMETSAT's OSI-SAF (OSI) retrieval algorithms. In the AMSR-E comparison, we use the enhanced NASA Team (NT2) algorithm instead of NT. Moreover, OSI SIC are not available based on AMSR-E data. An overview of the algorithms that we compare is given in Table II. All algorithms use a set of brightness temperature values—so-called tie points—that account for 0% and 100% ice concentration. These tie points have been derived from observations of different surface types such as open water and sea ice separately for each of the algorithms. Tie points represent typical radiometric signatures of these surface types. However, these signatures may vary considerably due to temperature changes, ice and snow property changes, and water content in the atmospheric column between the surface and the radiometer onboard a satellite. These variations can result in SIC biases and differences among the different algorithms.

NT uses 19 and 37 GHz Tb values to compute Tb polarization ratios (PRs) and gradient ratios (originally described in [25], [26]). The main SIC information comes from PR at 19 GHz. NT SIC has a grid resolution of 25 km × 25 km for SSM/I.

NT2 is an enhancement of the NT algorithm that has been designed to mitigate some of the problems inherent to NT [27]. In addition, 19 and 37 GHz channels, it uses 85 GHz (SSM/I) or 89 GHz (AMSR-E) Tb values to compute Tb PRs and gradient ratios. The main SIC information again comes from PR at 19 GHz. The other channels included mitigate the influence of different ice types and layering in the snow that caused problems with NT. A weather correction is applied that uses a catalogue of simulated SIC depending on standard atmospheric states. NT2 SIC has a grid resolution of 12.5 km × 12.5 km for AMSR-E and 25 km × 25 km for SSM/I.

For Antarctica, BST utilizes vertically polarized Tb values measured by the 19 and 37 GHz channels [28], [29]. The BST

algorithm interpolates between Tb value pair clusters forming for 0% and 100% SIC in Tb space. BST SIC has a grid resolution of 12.5 km × 12.5 km for AMSR-E and 25 km × 25 km for SSM/I.

OSI SIC [30], [31] are retrieved from a hybrid algorithm based on BST and the Bristol algorithm [32]. It uses Tb values measured by the 19- and 37-GHz channels. Instead of a weather filter, OSI incorporates an atmospheric correction through the use of a radiative transfer model. OSI SIC has a grid resolution of 10 km × 10 km for SSM/I.

ASI uses 85 GHz (SSM/I), 91 GHz (SSMIS), and 89 GHz (AMSR-E) Tb polarization difference to calculate SIC from tie points for 0% and 100% ice concentration [33], [22]. Using the higher frequency Tb measurements leads to an increased spatial resolution. As a tradeoff, these channels are more sensitive to influences from atmospheric cloud liquid water and water vapor on Tb [34]. ASI SIC has a grid resolution of 6.25 km × 6.25 km for AMSR-E and 12.5 km × 12.5 km for SSM/I.

Except OSI, the SIC retrieval algorithms use the gradient ratio of vertically polarized 19 and 37 GHz Tb values to filter out spurious SIC over open water [26], [35]. A second weather filter involves vertically polarized 19- and 22-GHz (AMSR-E: 23 GHz) Tb values. These weather filters reduce atmospheric effects from the atmospheric water content, however, they also limit detection of low SIC and of SIC associated with new ice. In addition, an increase in atmospheric water can also lead to erroneously increased SIC. This increase is more pronounced for low SIC [36].

For AMSR-E, NT2, and BST, data were obtained from the National Snow and Ice Data Center (NSIDC) as part of the *AMSR-E/Aqua Daily L3 12.5 km Brightness Temperature, SIC, and Snow Depth Polar Grids data set* [40]. The ASI SIC used here originates from a reprocessing of the AMSR-E Tb time series until 2011. This data set is available from the Integrated Climate Data Center at the University of Hamburg (ICDC, http://icdc.zmaw.de). Note that the tie points used for this reprocessing have been developed for the Arctic and have not yet been adapted to meet the perhaps different conditions in the Antarctic [22]. For SSM/I, NT and BST, were obtained from NSIDC, as part of the *SIC from Nimbus-7 SMMR and DMSP SSM/I-SSMIS Passive Microwave Data* [41] and the *Bootstrap SIC from Nimbus-7 SMMR and DMSP SSM/I-SSMIS data sets* [42]. OSI-SAF SIC [30] were downloaded from ICDC (http://icdc.zmaw.de), as were ASI SIC [43].

D. Colocation and Comparison Method

Ship OBS represent sea ice conditions on a scale on the order of 1 km for a defined time. An average speed of four knots (about 7 km/h) is a reasonable assumption, if a ship crosses the sea ice cover during navigable sea ice conditions. Therefore, during one day, a ship is able to transit a distance of 150–200 km, which corresponds to 12–16 grid cells with 12.5 km resolution; during light ice conditions, the ship's speed and the distance traveled are accordingly larger. In contrast, PM SIC are daily averages. Data from several satellite overpass from different times of one day are combined into one PM SIC value. In addition, this PM SIC value represents sea ice conditions on a scale on the order of 10–50 km. Temporal and spatial scales

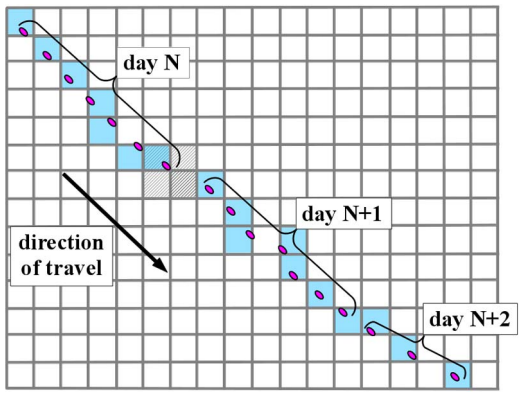

Fig. 1. Scheme of the colocation method. See text for explanation.

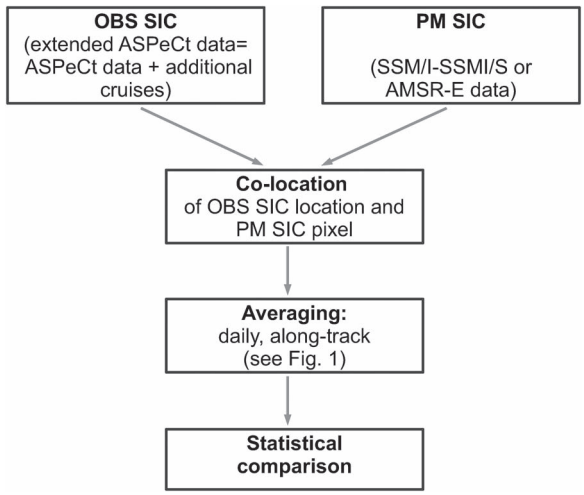

Fig. 2. Analysis structure in this paper shown in flowchart form.

between OBS SIC and PM SIC are therefore quite different. It can be expected that OBS SIC is more variable than PM SIC, and a direct comparison of OBS SIC and PM SIC as they are is therefore questionable. As a solution of this caveat, we suggest to compare both data sets on a daily along-track average basis to align the different spatial and temporal scales of OBSs with the satellite data.

Throughout this paper, the colocation of OBS SIC with PM SIC is as follows: PM SIC are transformed onto a Cartesian grid (see Fig. 1). The distance to the center of the surrounding PM SIC grid cells is computed for each OBS SIC location, as shown in Fig. 1 by the hatched pixels for the last ship position on day N. The grid cell with the minimum distance is selected for the comparison, which is shown by the blue-colored pixels in Fig. 1. After the colocation, we compute the average along-ship track OBS SIC for all observations of one day ($\mathrm{N_{day}}$) and the average PM SIC for all $\mathrm{N_{day}}$ colocated PM SIC grid cells (see Fig. 2).

For a single point in time, we require all data sets to provide a value: if one of the data sets has a missing value, the specific point in time is not used for the comparison. For the SSM/I comparison, this procedure yields a period from December 1991 until February 2009 with 21625 OBS/PM SIC data pairs. Limits in the comparison time frame are due the 85 GHz channels only being reliably available from the start of DMSP F-11 in December 1991 (see Section II-B) and from

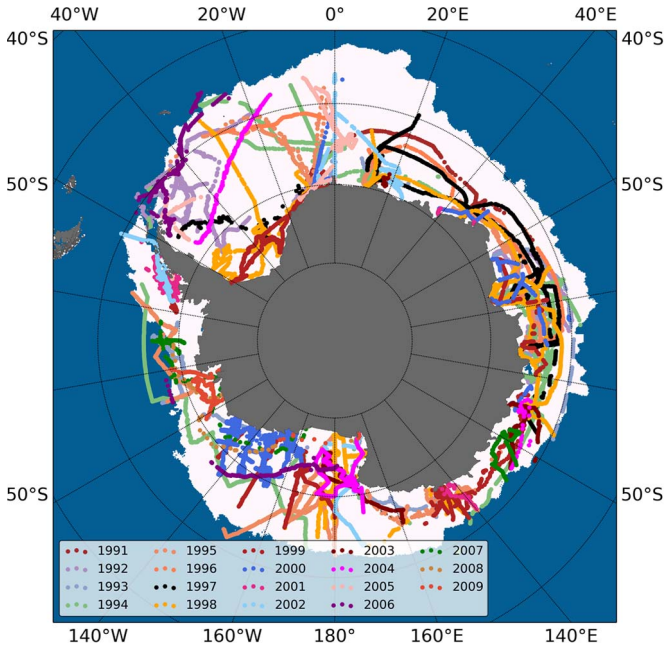

Fig. 3. ASPeCt ship tracks (OBS) during the SSM/I comparison period (1991–2009) projected onto an ASI sea ice extent map of September 7, 2005.

the reprocessed OSI data ending in 2009. For the AMSR-E comparison, we investigate the period from August 2002 until December 2010 with 3871 OBS/PM SIC data pairs. For the daily along-track averaging, cases with $N_{day} < 3$ were discarded. This led to 1132 SIC daily averages in total to be used for our SSM/I comparison, 516 of which were from the winter months (April–September) and 616 from the summer months (October–March). For the AMSR-E comparison, we obtain 320 SIC daily averages, 84 of which were from the winter months and 236 from the summer months.

E. Statistical Comparison

We assess the performance of the different PM SIC methods compared with OBS SIC by calculating the correlation coefficient, the RMSD and the bias, which we define here as the mean difference between PM SIC and OBS SIC. Since SIC data are not normally distributed (see in Figs. 4, 7, and 9), we calculate Spearman rank correlation coefficients (denoted as r from this point onward) instead of Pearson's product moment correlation coefficients for our comparison of PM SIC and OBS SIC.

III. Results

A. SSM/I Period

The tracks of the ships from which the ice concentration data used in our comparison are shown in Fig. 3. Positions are overlaid onto an ASI sea ice extent map for September 7, 2005 based on SSM/I data. Due to the advantage of a long comparison period, SIC were collected all around Antarctica. Only an area between 0° and 30° E and 60° and 55° S shows no ship tracks. This area is usually covered by sea ice only at the end of winter.

The distribution of daily mean SIC in tenth of 100% for OBS, ASI, OSI, NT, and BST shows only little differences among

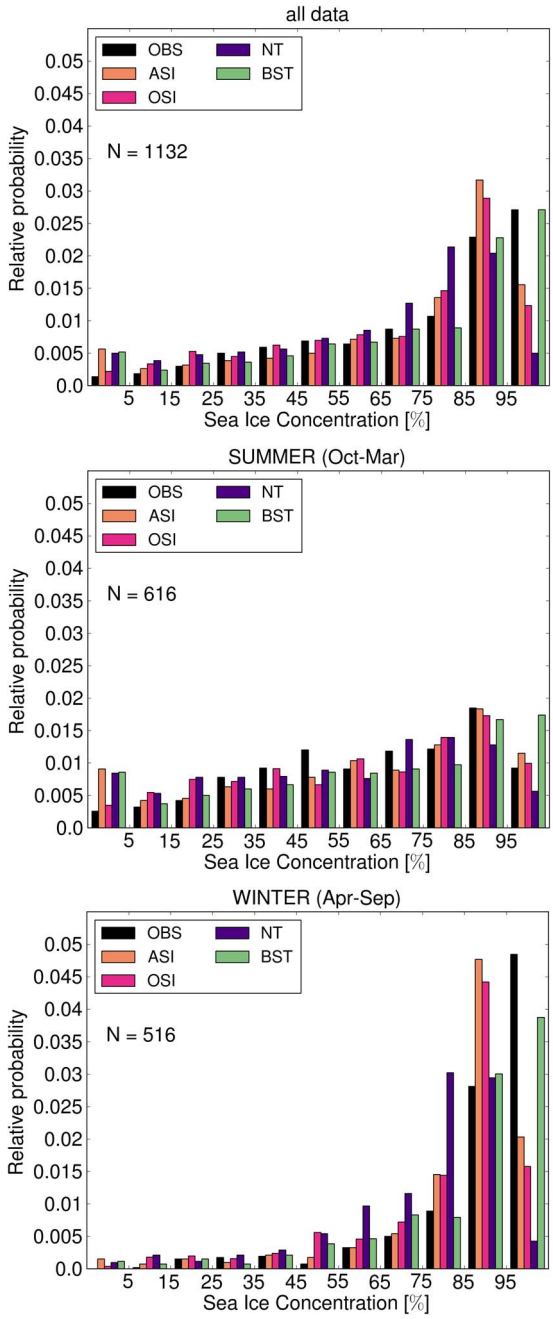

Fig. 4. Histogram of daily mean along-ship track SIC that are used in the SSM/I comparison. Top panel: all data; middle panel: data from the summer months (October–March); lower panel: data from the winter months (April–September). Legends indicate the different algorithms. In each panel, the number of days N used in the comparison is shown.

the compared SIC algorithms in the 5–15% to 55–65% bins (see Fig. 4, upper panel). In other bins in the histogram, several differences exist. In general, the PM data tend to overestimate SIC values below 25%, whereas for high SIC values individual differences occur. In the 75–85%-bin, NT tends to overestimate SIC. In the $>$ 95%-bin, aside from the BST, all PM data sets underestimate OBS SIC. During summer, differences only exist in the very low SIC regime (0–5%-bin) and for very high SIC ($>$ 95%-bin) (see Fig. 4, middle panel). During winter, however, differences are more pronounced: NT strongly overestimates OBS in the 75–85%-bin, ASI and OSI overestimate

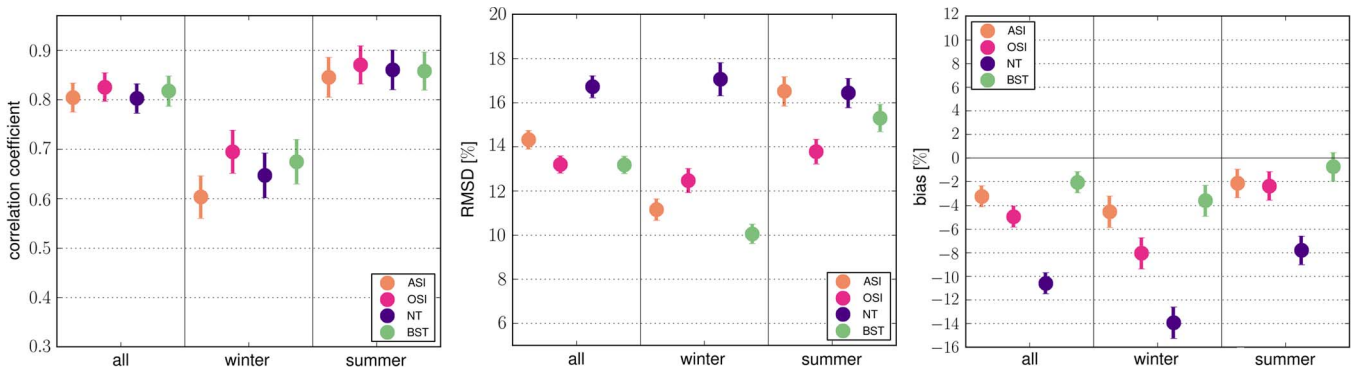

Fig. 5. Statistics of the comparison of daily mean along-ship track average SIC from PM and OBS for SSM/I. Left panel: correlation coefficient; middle panel: RMSD; right panel: bias.

TABLE III
SUMMARY OF STATISTICAL NUMBERS IN THE SSM/I COMPARISON

		BST	OSI	ASI	NT
	CC	0.82 ± 0.03	0.83 ± 0.03	0.80 ± 0.03	0.80 ± 0.03
all data	**RMSD**	13.2 ± 0.4	13.2 ± 0.4	14.3 ± 0.4	16.7 ± 0.5
	bias	-2.0 ± 0.9	-5.0 ± 0.9	-3.2 ± 0.9	-10.6 ± 0.9
	CC	0.86 ± 0.04	0.87 ± 0.04	0.85 ± 0.04	0.86 ± 0.04
summer	**RMSD**	15.3 ± 0.6	13.8 ± 0.6	16.5 ± 0.7	16.4 ± 0.7
	bias	-0.7 ± 1.2	-2.4 ± 1.2	-2.1 ± 1.2	-7.8 ± 1.2
	CC	0.67 ± 0.04	0.70 ± 0.04	0.60 ± 0.05	0.65 ± 0.04
winter	**RMSD**	10.1 ± 0.4	12.5 ± 0.5	11.2 ± 0.5	17.1 ± 0.8
	bias	-3.6 ± 1.3	-8.1 ± 1.3	-4.5 ± 1.3	-13.9 ± 1.3

OBS in the 85–95%-bin and in the $>95\%$-bin, only BST comes close to the number of SIC values accounted for by OBS (see Fig. 4, lower panel).

Fig. 5 and Table III summarize the statistical comparison between the individual PM SIC and OBS SIC for the SSM/I data. The differences in the correlation coefficients (CC) lie within the uncertainty of the correlation: BST: $CC = 0.82 \pm 0.03$, OSI: $CC = 0.83 \pm 0.03$, ASI: $CC = 0.80 \pm 0.03$, NT: $CC = 0.80 \pm 0.03$. The uncertainty is estimated separately for each satellite product by a Monte Carlo simulation of the data and 1000 repeated calculations of CC. During winter, correlations drop down to $CC = 0.67 \pm 0.04$ for BST, $CC = 0.70 \pm 0.04$ for OSI, $CC = 0.60 \pm 0.05$ for ASI, and $CC = 0.65 \pm 0.04$ for NT, respectively. During summer, correlations slightly increase, although the different values for r usually stay within the uncertainty range (BST: $CC = 0.86 \pm 0.04$, OSI: $CC = 0.87 \pm 0.04$, ASI: $CC = 0.85 \pm 0.04$, NT: $CC = 0.86 \pm 0.04$). RMSD and bias show larger differences between the satellite data. Notably, NT shows high values for bias and RMSD: the bias is at least -10% in all data and almost -14% in the summer months, the RMSD is more than 16% in all seasons. RMSD values for OSI range between 12.5% in winter and 13.8% in summer. ASI shows a greater RMSD value in summer than winter. BST has a very low bias, only increasing to -3.6% in the winter months. The bias is generally slightly lower for ASI than for OSI. Both ASI and OSI range between the minimum values for BST and the maximum values for NT. Aside from NT, all algorithms show a lower winter than summer bias, but NT's winter bias increases to 17.1%.

B. AMSR-E Period

The positions of OBS used for the AMSR-E comparison are overlaid onto a AMSR-E-based ASI sea ice extent map for September 7, 2005 (see Fig. 6). Due to the limited number of years available for this comparison, OBS SIC were only collected in the Weddell Sea, around the Antarctic Peninsula, Bellingshausen Sea, Amundsen Sea, Ross Sea, and the South Indian Ocean.

The distribution of daily mean SIC for OBS, ASI, NT2, and BST shows almost no discrepancies among the compared SIC algorithms in the 5–15% to 55–65% bins (see Fig. 7, upper panel). The NT2 algorithm detects more sea ice in the $>95\%$-bin than the other SIC algorithms. Furthermore, all algorithms overestimate very sparse ice concentration of OBS. The overestimation of $>95\%$ OBS SIC by PM data is most pronounced in summer, particularly for NT2 (see Fig. 7, middle panel). Note that OBS SIC have a maximum probability in the 85–95%-bin with a following decrease in the $>95\%$-bin. This is not matched by the PM data. In contrast to NT2's overestimation of SIC $>95\%$, NT2 underestimates the number of SIC values falling into the 85–95%-bin. ASI and BST also show this discrepancy, but not as pronounced as NT2. In the summer months, there is a peak of OBS SIC in the 45–55%-bin that is not reproduced by PM SIC. During winter, NT2 again overestimates very high ice concentration and underestimates the number of observations in the bin below, the 85–95%-bin (see Fig. 7, lower panel). However, due to the small number of data pairs during the winter months, these differences are not as significant as in summer.

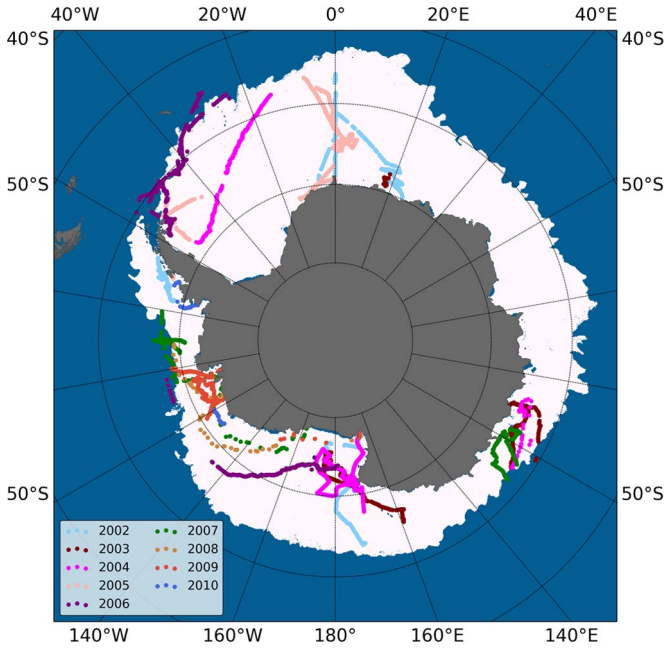

Fig. 6. ASPeCt ship tracks (OBS) during the AMSR-E comparison period (2002–2009) projected onto an ASI sea ice extent map of September 7, 2005.

Fig. 8 and Table IV summarize the statistical comparison between the individual PM SIC and OBS SIC for the AMSR-E period. In contrast to the SSM/I comparison, correlation coefficients are slightly higher (BST: CC $= 0.85 \pm 0.06$, ASI: CC $= 0.84 \pm 0.06$, NT: CC $= 0.84 \pm 0.06$), but with a concurrent increase of the uncertainty in r, which is due to the lower number of data pairs for the AMSR-E period. Correlation coefficients in summer increase even further to almost 0.9 for all PM SIC, whereas they decrease in winter to about 0.5 for ASI and 0.6 for BST. As for SSM/I, we recognize the same tendency for RMSD: summer values are greater than winter values. While there is only very little bias for BST and ASI in both summer and winter, NT2 has a pronounced summer bias, almost twice as large as the 5% bias in winter.

C. Sensor Comparison

In a third comparison, we assess the performance of two PM SIC retrieval algorithms that are applicable to SSM/I and AMSR-E data. We choose BST and ASI for this comparison, as they tend to provide the best results in the previous comparisons. The positions of OBS used for this comparison are identical to those shown in Fig. 6.

The distribution of daily mean SIC for OBS, ASI-AMSR-E, ASI-SSM/I, BST-AMSR-E, and BST-SSM/I shows the largest differences for both seasons in the high SIC regime (SIC $> 85\%$) (Fig. 9, upper panel). These differences are more pronounced in winter months. However, winter contains a much lower number (N $= 86$) of data pairs than summer (N $= 320$). In addition, PM SIC tend to overestimate very low OBS SIC ($< 5\%$). This is more pronounced in summer, which depicts the season with a higher fraction of open water within the sea ice cover. Contrary to this, sea ice is often wet in this season and thus difficult to be detected in PM data. It seems that navigating through very open ice areas during summer (and thus causing a low bias) is outweighed by the effect of wet ice being invisible for PM but visible for OBS.

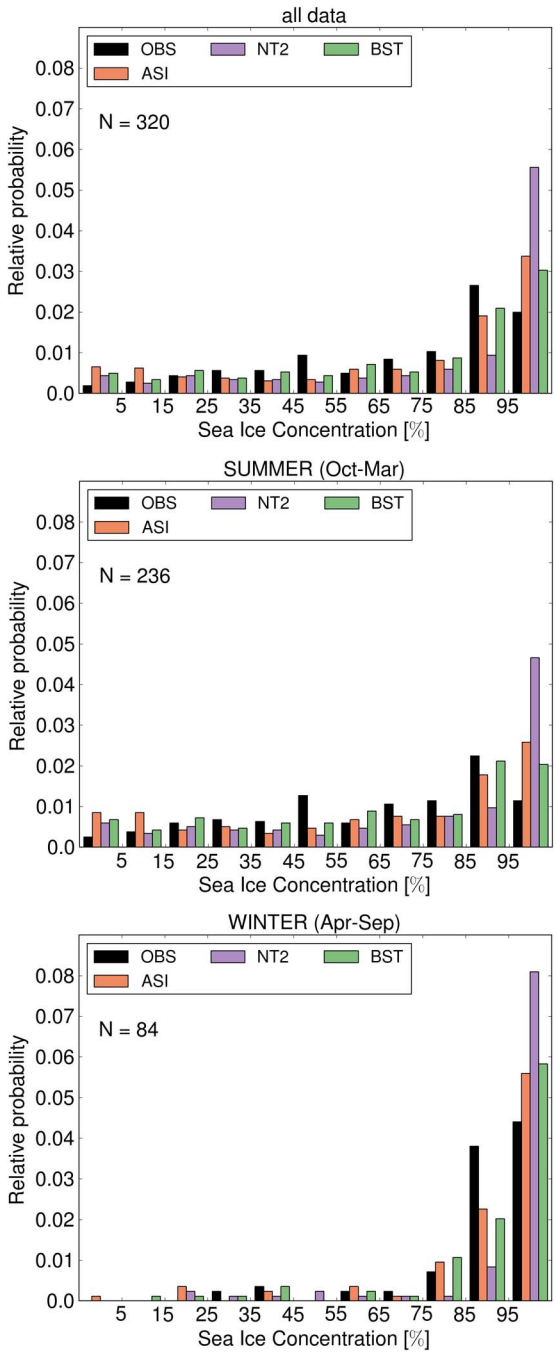

Fig. 7. Same as Fig. 4 but for the AMSR-E comparison.

Fig. 10 and Table V summarize the statistical comparison between the individual PM SIC and OBS SIC for the sensor comparison, covering the years 2002–2010. There is no significant difference in accuracy between either different algorithms applied to the same sensor data or the same algorithm applied to different sensor data. A few tendencies, however, are recognizable: considering all statistical numbers, BST shows more consistency to OBS with lower RMSD values, a better correlation in winter, and a near-zero bias. SIC based on AMSR-E data tend to agree better with OBS SIC than SIC

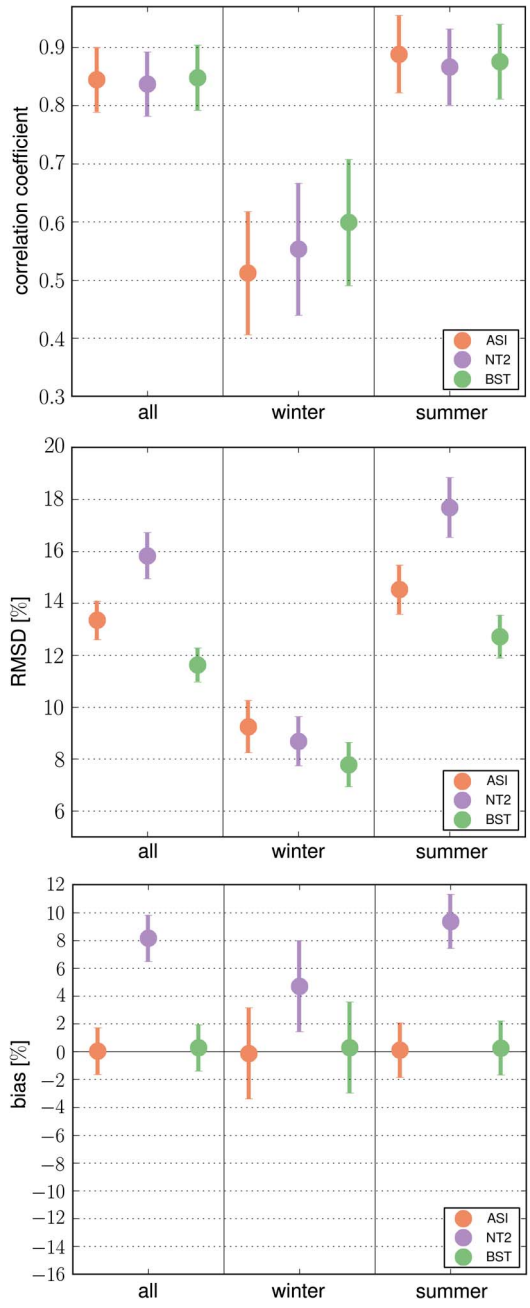

Fig. 8. Same as Fig. 5 but for the AMSR-E comparison.

based on SSM/I data. Similar to the other two comparisons, RMSD values and correlations are reduced during winter.

IV. Discussion

In the previous section, we have presented the results of our comparison between OBS SIC and colocated satellite PM SIC based on several algorithms. The results turned out to be quite different for the different retrieval algorithms used. However, are the obtained results sufficient to give a recommendation, about which SIC retrieval algorithm is best to use based on a comparison with OBS SIC? This is going to be discussed in the following section.

Retrieval algorithms for SIC differ in how ice concentration values are derived from PM-measured brightness temperatures.

TABLE IV
Summary of Statistical Numbers in the AMSR-E Comparison

		BST	ASI	NT2
all data	CC	0.85 ± 0.06	0.84 ± 0.06	0.84 ± 0.06
	RMSD	11.6 ± 0.7	13.3 ± 0.7	15.8 ± 0.9
	bias	0.3 ± 1.7	0.0 ± 1.7	8.1 ± 1.7
summer	CC	0.88 ± 0.06	0.89 ± 0.07	0.87 ± 0.06
	RMSD	12.7 ± 0.8	14.5 ± 0.9	17.7 ± 1.2
	bias	0.3 ± 2.0	0.1 ± 2.0	9.4 ± 2.0
winter	CC	0.60 ± 0.11	0.51 ± 0.11	0.55 ± 0.11
	RMSD	7.8 ± 0.8	9.3 ± 1.0	8.7 ± 0.9
	bias	0.3 ± 3.3	-0.1 ± 3.3	4.7 ± 3.3

They use different combinations of different channels that have distinct characteristics, e.g., the frequencies differ in their sensitivity to atmospheric water vapor and liquid water content, both of which influence the radiation received at the radiometer. Additionally, the algorithms need to use tie points that represent typical radiometric signatures of ice and open water. These tie points are usually derived from satellite measurements and contain the influence of the mean atmospheric state. In atmospheric conditions that are different from this mean atmospheric state, the derived tie points will lead to biased SIC values.

While the open water tie point is generally influenced by atmospheric variability, the ice tie point is influenced by sea ice emissivity variations. Therefore, SIC retrieved for very open ice conditions are most sensitive to the choice of the open water tie point and high ice concentrations are sensitive to surface processes [36]. Generally, one seeks for a high signal-to-noise ratio when choosing the tie points aiming for a high sensitivity in retrieving PM SIC. Open water tie points are usually set very close to a minimum brightness temperature or maximum brightness temperature polarization difference or ratio, which corresponds to a clear sky, dry atmosphere, and a smooth water surface. The use of weather filters reduces the influence of atmospheric water and wind on the emissivity of the open water surface. However, this can lead to a cutoff of low SIC values. Only the reprocessed OSI data provide SIC without a cutoff by using dynamic tie points that, for instance, minimize the effect of atmospheric emission [31].

Improvements of AMSR-E data over SSM/I data that are relevant for this comparison include higher spatial resolution at all scanned frequencies and a wider swath width. The wider swath width leads to more brightness temperature measurements that are used to calculate a daily-mean SIC value from the specific algorithm and, thus, can increase the significance of a calculated daily-mean SIC value during static ice conditions. In the MIZ, this can still lead to a smearing of the ice edge, particularly under very dynamic ice conditions, e.g., during the passing of a cyclone. When retrieving geophysical parameters such as the SIC, the higher spatial resolution of AMSR-E can reduce uncertainties. Such uncertainties may partly be due to smaller spatial variability of differently emitting surfaces, e.g., different ice types, snow cover, or water surfaces. These different surface types particularly influence the use of mixing algorithms [44],

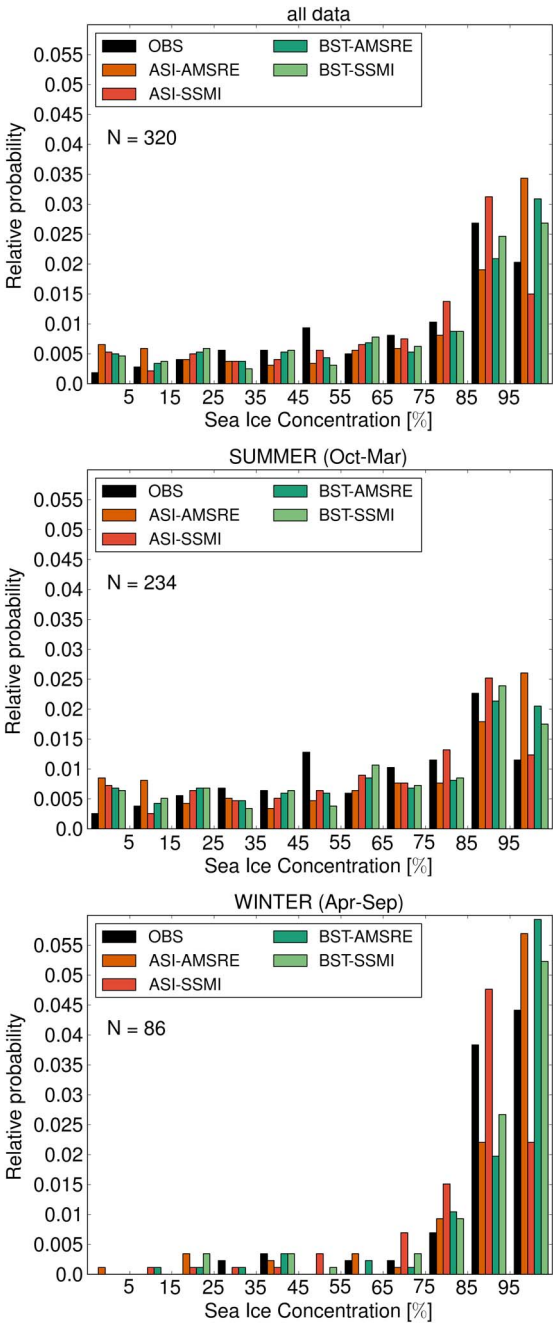

Fig. 9. Same as Fig. 4 but for the sensor comparison.

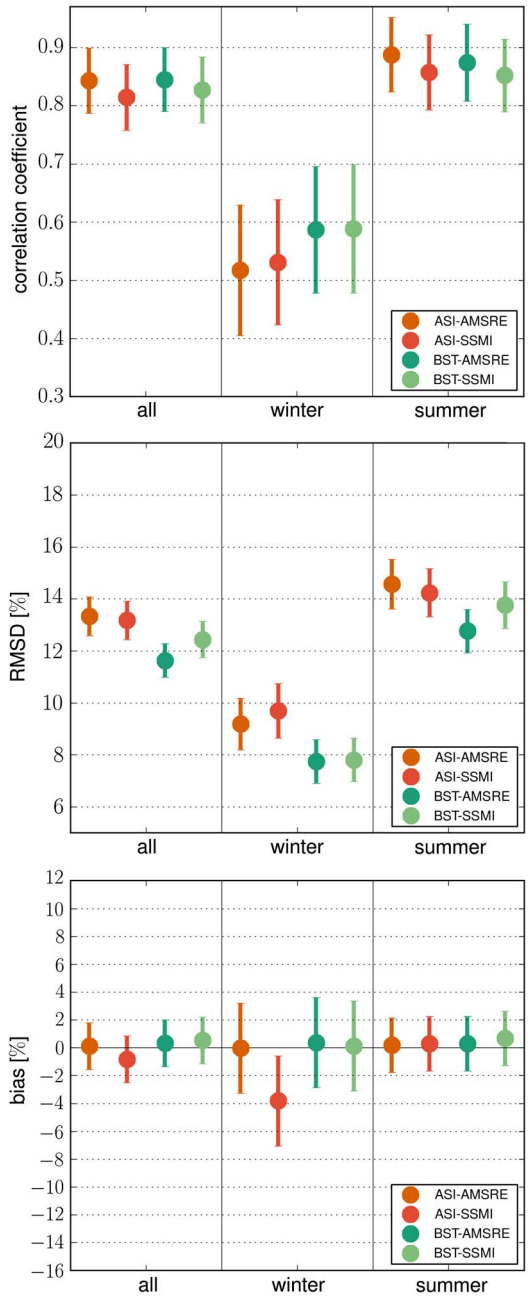

Fig. 10. Same as Fig. 5 but for the sensor comparison.

particularly in the MIZ, where the higher spatial resolution of the AMSR-E sensor allows for a more precise detection of the ice edge [4]. In our case, with a finer spatial resolution, one should get a better representation of leads and open water areas in high ice concentration regimes, i.e., of SIC in the range $> 85\%$. The same applies to using 85 GHz (SSM/I), 91.655 GHz (SSMIS), or 89 GHz (AMSR-E) data compared with using the standard frequencies 19 GHz and 37 GHz as was demonstrated for SSM/I by Kaleschke *et al.* [33] and Kern [8].

Sea ice continuously changes its emissivity from its initial growth stage to thick first-year ice [45]–[47]. In particular, thin sea ice with thicknesses below about 20 cm often has lower microwave emissivities than thicker sea ice or snow covered sea ice. Therefore, PM SIC retrieval algorithms can underestimate SIC in areas of thin sea ice by an unknown amount [22], [29], [48].

We have shown SIC values in the histograms (see Figs. 4, 7, and 9) sorted in bins for 0%–5%, 5%–15%, 15%–25% $\cdots$ 85%–95%, and 95%–100% SIC according to the increments used in the ASPeCt protocol when observing SIC. Due to the daily averaging, we have values that differ from this quantization into 10% increments. In order to keep this quantization visible and to also consider the accuracy of the ASPeCt observations, we used as division of PM SIC the same increments that were used in the ASPeCt protocol. However, the differences between PM SIC and OBS SIC shown in the histograms (see Figs. 4, 7, and 9) are highest in neighboring bins: 85–95%

TABLE V
SUMMARY OF STATISTICAL NUMBERS IN THE SENSOR COMPARISON FOR ASI SIC AND BST SIC

		BST/AMSR-E	BST/SSMI	ASI/AMSR-E	ASI/SSMI
	CC	0.84 ± 0.06	0.83 ± 0.05	0.84 ± 0.06	0.81 ± 0.06
all data	**RMSD**	11.6 ± 0.7	12.4 ± 0.7	13.3 ± 0.7	13.2 ± 0.7
	bias	0.3 ± 1.7	0.5 ± 1.7	0.1 ± 1.7	-0.8 ± 1.7
	CC	0.87 ± 0.07	0.85 ± 0.06	0.89 ± 0.06	0.86 ± 0.06
summer	**RMSD**	12.8 ± 0.8	13.8 ± 0.9	14.6 ± 1.0	14.2 ± 0.9
	bias	0.3 ± 2.0	0.7 ± 2.0	0.2 ± 2.0	0.3 ± 2.0
	CC	0.59 ± 0.11	0.59 ± 0.11	0.52 ± 0.11	0.53 ± 0.11
winter	**RMSD**	7.7 ± 0.8	7.8 ± 0.8	9.2 ± 1.0	9.7 ± 1.0
	bias	0.4 ± 3.2	0.1 ± 3.2	0.0 ± 3.2	-3.8 ± 3.2

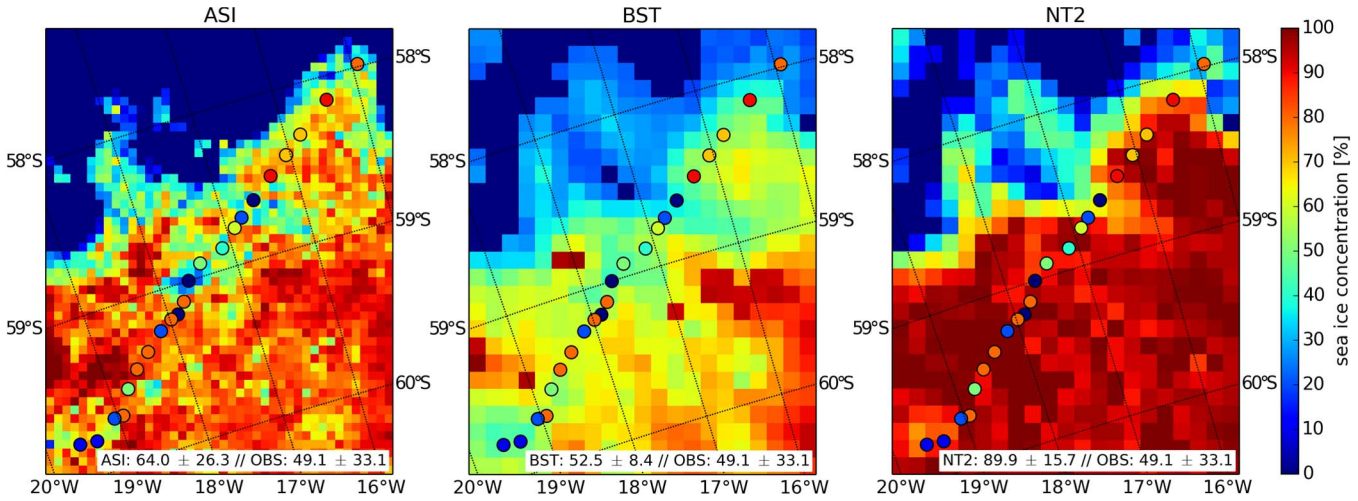

Fig. 11. Example of a daily track crossing the sea ice edge in the Weddell Sea on November 14, 2004. SIC based on AMSR-E are shown for (left to right): ASI (grid resolution: 6.25 km), BST (grid resolution: 12.5 km), and NT2 (grid resolution: 12.5 km). The daily mean and the daily standard deviation for OBS, ASI, BST, and NT2 are 49.1% ± 33.1%, 64.0% ± 26.3%, 52.5% ± 8.4%, and 89.9% ± 15.7%, respectively.

and $> 95\%$. We cannot exclude that using a different binning such as 0%–10%, 10%–20% $\cdots$ 90%–100% might change the results of the histograms. However, we are confident that the main results of our study, which are summarized in Figs. 5, 8, and 10, will not change due to a different binning.

The number of data pairs differs for the different seasons. In particular in the AMSR-E comparison, only 25% of the data fall into winter months. However, due to the number of data points, with at least three observations required for a daily-average value, the results for the winter season can still be regarded as significant.

OBSs are often biased toward thin ice regions, because ships tend to avoid thick and ridged ice areas and rather follow leads and openings [14]. Ridged ice areas can correspond to regions of convergent ice motion and, thus, high ice concentrations, whereas regions with many leads and openings correspond to divergent ice motion and can have lower ice concentrations. Therefore, we cannot exclude that OBS SIC are slightly biased toward low ice concentrations, particularly during summer when leads and openings do not freeze over. At the same time, however, PM SIC might also be biased low in areas with leads and openings due to the higher fraction of thin ice; this effect would be more pronounced during winter though.

In this paper, we do not distinguish between different regions and potentially different sea ice regimes. The Bellingshausen Sea, for instance, is known for more compact, thicker, and less mobile first year sea ice [49]. Distinguishing between different regions could help to understand where different algorithms have their strengths or limitations. However, this is not intended in this paper, which rather looks at the performance of different algorithms compared with a long-term basin-scale ground-truth data set. Due to the number of observations, we regard our conclusion as robust and being generally true for the Antarctic sea ice as a whole. If we had looked at different ice types or had tried to distinguish between different regions, the number of data pairs would have dropped substantially and the results would have been less robust.

In all three comparisons shown in this paper, BST SIC has the closest correspondence to OBS SIC, both for SSM/I and AMSR-E data. However, the higher resolution of the ASI algorithm can provide more information than algorithms using the lower frequency channels for their retrievals. One aspect is the higher spatial variability that is more accurately reproduced by ASI (see Fig. 11). This is an advantage for navigational purposes and for mesoscale process studies [33].

V. Conclusion

We compare passive microwave (PM)-derived SIC with those from OBS, and we focus on different retrieval algorithms that are based on SSM/I-SSMIS and AMSR-E measurements. OBS SIC are collected according to the ASPeCt protocol. We assess the quality of PM SIC by calculating correlation coefficients, RMSDs, and biases with respect to OBS SIC. In contrast to previous studies, we apply a different method to compare the colocated OBS SIC with PM SIC to account for the different temporal and spatial scales between locally observed SIC on a scale on the order of 1 km and those derived with PM sensors on a scale on the order of 10 km. We use daily along-ship track average SIC.

According to our analysis, we can rank the investigated retrieval algorithms: in the SSM/I comparison, BST SIC reveal a high correlation, the smallest RMSD, and a very low negative bias compared with OBS SIC, and thus, BST performs best out of our choice of algorithms. EUMETSAT's OSI-SAF (OSI) SIC show a similar RMSD, but a larger absolute bias than BST, and thus, OSI ranks as second best algorithm. ASI SIC shows a significantly larger RMSD and also a very low bias. NASA Team (NT) SIC, while providing a similarly high correlation, clearly perform the worst out of our choice of algorithms with the highest RMSD values and a significantly larger bias of -10% or more. In the AMSR-E comparison, BST SIC reveal the smallest RMSD, and a near zero bias compared with OBS SIC and thus perform the best out of our choice of algorithms. ASI SIC show a significantly larger RMSD and also a near zero bias. Like NT in the SSM/I-SSMIS comparison, enhanced NASA Team (NT2) SIC provide a similarly high correlation, but perform the worst out of our choice of algorithms with RMSD values, except for winter, above those for ASI SIC and a significantly larger bias of roughly 8%.

Due to the length of the different PM SIC time series, we have an overlap of OBS SIC and PM SIC that leads to periods of investigation spanning 1991–2009 for SSM/I data, a total of 21 625 data pairs, and spanning 2002–2010 for AMSR-E data, a total of 3871 data pairs. To our knowledge, there has not been a comparison with this number of OBSs of SIC with PM-derived SIC, and we therefore regard our results as robust. This paper is an important contribution to SIC evaluation in the *in situ* data sparse region of the Southern Ocean.

Acknowledgment

The authors would like to thank the National Snow and Ice Data Center in Boulder, Colorado, USA, and the JAXA EORC (Earth Observation Research Center) in Tokyo, Japan, for providing SSM/I, SSMIS, and AMSR-E data. The authors acknowledge the support from the International Space Science Institute, Bern, Switzerland. They are grateful to ice observers aboard the Antarctic research voyages that contributed data for the ASPeCt data used in this paper. The authors also thank A. H. Tekeli (now at Zirve Univ., Gaziantep, Turkey), S. F. Ackley (now at Univ. San Antonio), B. Ozsoy-Cicek (now at Technical University Istanbul), and S. Willmes (Univ. Trier) for providing additional ship-based observation to extend the ASPeCt data.

References

[1] A. Stössel, "Employing satellite-derived sea ice concentration to constrain upper-ocean temperature in a global ocean GCM," *J. Climate*, vol. 21, no. 17, pp. 4498–4513, Sep. 2008.

[2] P. Uotila *et al.*, "Relationships between Antarctic cyclones and surface conditions as derived from high-resolution numerical weather prediction data," *J. Geophys. Res.*, vol. 116, no. D7, pp. D07109-1–D07109-14, Apr. 2011.

[3] C. J. Donlon *et al.*, "The operational sea surface temperature and sea ice analysis (OSTIA) system," *Remote Sens. Environ.*, vol. 116, pp. 140–158, Jan. 2012.

[4] A. Worby and J. Comiso, "Studies of the Antarctic sea ice edge and ice extent from satellite and ship observations," *Remote Sens. Environ.*, vol. 92, no. 1, pp. 98–111, Jul. 2004.

[5] M. A. Knuth and S. F. Ackley, "Summer and early-fall sea-ice concentration in the Ross Sea: Comparison of *in situ* ASPeCt observations and satellite passive microwave estimates," *Ann. Glaciol.*, vol. 44, no. 1, pp. 303–309, Nov. 2006.

[6] B. Ozsoy-Cicek, H. Xie, S. F. Ackley, and K. Ye, "Antarctic summer sea ice concentration and extent: Comparison of ODEN 2006 ship observations, satellite passive microwave and NIC sea ice charts," *Cryosphere*, vol. 3, no. 1, pp. 1–9, 2009.

[7] A. E. Tekeli, S. Kern, S. F. Ackley, B. Ozsoy-Cicek, and H. Xie, "Summer Antarctic sea ice as seen by ASAR and AMSR-E and observed during two IPY field cruises: A case study," *Ann. Glaciol.*, vol. 52, no. 57, pp. 327–336, May 2011.

[8] S. Kern, "A new method for medium-resolution sea ice analysis using weather-influence corrected special sensor microwave/imager 85 GHz data," *Int. J. Remote Sens.*, vol. 25, no. 21, pp. 4555–4582, Nov. 2004.

[9] G. Heygster *et al.*, "PELICON: Project for estimation of long-term variability of ice concentration," Bremen, Germany, Tech. Report Contract EV5V-CT93-0268(DG 12 DTEE), 1996.

[10] S. Kern, "A new algorithm to retrieve the sea ice concentration using weather corrected 85 GHz SSM/I measurements," in *Berichte aus dem Institut für Umweltphysik*, vol. 6. Berlin, Germany: Logos-Verlag, 2001.

[11] S. Kern and G. Heygster, "Sea-ice concentration retrieval in the Antarctic based on the SSM/I 85.5 GHz polarization," *Ann. Glaciol.*, vol. 33, no. 1, pp. 109–114, Jan. 2001.

[12] B. Weissling, S. Ackley, P. Wagner, and H. Xie, "EISCAM—Digital image acquisition and processing for sea ice parameters from ships," *Cold Regions Sci. Technol.*, vol. 57, no. 1, pp. 49–60, Jun. 2009.

[13] S. Nihashi, K. I. Ohshima, M. O. Jeffries, and T. Kawamura, "Sea-ice melting processes inferred from ice-upper ocean relationships in the Ross Sea, Antarctica," *J. Geophys. Res.*, vol. 110, no. C2, pp. C02002-1–C02002-12, Feb. 2005.

[14] B. Ozsoy-Cicek, S. F. Ackley, A. Worby, H. Xie, and J. Lieser, "Antarctic sea-ice extents and concentrations: Comparison of satellite and ship measurements from international polar year cruises," *Ann. Glaciol.*, vol. 52, no. 57, pp. 318–326, May 2011.

[15] A. P. Worby, I. Allison, V. Dirita, and C. Antarctic, "A technique for making ship-based observations of Antarctic sea ice thickness and characteristics," Antarctic CRC, Hobart, Australia, May 1999.

[16] A. P. Worby *et al.*, "Thickness distribution of Antarctic sea ice," *J. Geophys. Res.—Oceans*, vol. 113, no. C5, pp. C05S92-1–C05S92-14, May 2008.

[17] C. Haas *et al.*, "Regional variability of sea ice properties and thickness in the northwestern Weddell Sea obtained by in-situ and satellite measurements," in *The Expedition ANTARCTIC XXIII/7 of the Research Vessel Polarstern in 2006*, vol. 586, P. Lemke, Ed. Bremerhaven, Germany: Alfred Wegener Inst. Polar Marine Res., 2009, ser. Reports on Polar and Marine Research.

[18] J. Hollinger, R. Lo, G. Poe, R. Savage, and J. Peirce, *SSM/I User's Guide*. Washington, DC, USA: Naval Res. Lab., 1987.

[19] K. Tateyama and H. Enomoto, "Observation of sea-ice thickness fluctuation in the seasonal ice-covered area during 1992–99 winters," *Ann. Glaciol.*, vol. 33, no. 1, pp. 449–456, Jan. 2001.

[20] B. Yan and F. Weng, "Intercalibration between special sensor microwave imager/sounder and special sensor microwave imager," *IEEE Trans. Geosci. Remote Sens.*, vol. 46, no. 4, pp. 984–995, Apr. 2008.

[21] T. Kawanishi *et al.*, "The Advanced Microwave Scanning Radiometer for the Earth observing system (AMSR-E), NASDA's contribution to the EOS for global energy and water cycle studies," *IEEE Trans. Geosci. Remote Sens.*, vol. 41, no. 2, pp. 184–194, Feb. 2003.

[22] G. Spreen, L. Kaleschke, and G. Heygster, "Sea ice remote sensing using AMSR-E 89-GHz channels," *J. Geophys. Res.—Oceans*, vol. 113, no. C2, pp. C02S03-1–C02S03-14, Feb. 2008.

[23] J. Hollinger, J. Peirce, and G. Poe, "SSM/I instrument evaluation," *IEEE Trans. Geosci. Remote Sens.*, vol. 28, no. 5, pp. 781–790, Sep. 1990.
[24] N. Grumman, "Algorithm and Data User Manual (ADUM) for the Special Sensor Microwave Imager/Sounder (SSMIS)," Northrop Grumman Corp. Space Syst. Div., Azusa, CA, USA, Jul. 2002, Tech. Rep. contract No: F04710-00-C-0001.
[25] D. J. Cavalieri, P. Gloersen, and W. J. Campbell, "Determination of sea ice parameters with the Nimbus-7 SMMR," *J. Geophys. Res.—Atmos.*, vol. 89, no. D4, pp. 5355–5369, Jun. 1984.
[26] P. Gloersen and D. J. Cavalieri, "Reduction of weather effects in the calculation of sea ice concentration from microwave radiances," *J. Geophys. Res.—Oceans*, vol. 91, no. C3, pp. 3913–3919, Mar. 1986.
[27] T. Markus and D. J. Cavalieri, "An enhancement of the NASA Team sea ice algorithm," *IEEE Trans. Geosci. Remote Sens.*, vol. 38, no. 3, pp. 1387–1398, May 2000.
[28] J. C. Comiso, "SSM/I sea ice concentrations using the bootstrap algorithm," Goddard Space Flight Center, Greenbelt, MD, USA, NASA Ref. Publ. 1380, 1995.
[29] J. C. Comiso, D. J. Cavalieri, and T. Markus, "Sea ice concentration, ice temperature, and snow depth using AMSR-E data," *IEEE Trans. Geosci. Remote Sens.*, vol. 41, no. 2, pp. 243–252, Feb. 2003.
[30] EUMETSAT Ocean and Sea Ice Satellite Application Facility, Global Sea Ice Concentration Reprocessing Dataset 1978–2009 (v2, 2011), 2011, Norwegian and Danish Meteorological Institutes. [Online]. Available: osisaf.met.no
[31] S. Eastwood, K. R. Larsen, T. Lavergne, E. Nielsen, and R. Tonboe, "Global sea ice concentration reprocessing—Product user manual, Product OSI-409," EUMETSAT, Darmstadt, Germany, Oct. 2011, SAF/OSI/CDOP/met.no/TEC/MA/138, Tech. Rep. Ver. 1.3. [Online]. Available: http://www.osi-saf.org
[32] D. Smith, "Extraction of winter total sea-ice concentration in the Greenland and Barents Seas from SSM/I data," *Int. J. Remote Sens.*, vol. 17, no. 13, pp. 2625–2646, 1996.
[33] L. Kaleschke *et al.*, "SSM/I sea ice remote sensing for mesoscale ocean-atmosphere interaction analysis," *Can. J. Remote Sens.*, vol. 27, no. 5, pp. 526–537, Oct. 2001.
[34] C. Oelke, "Atmospheric signatures in sea-ice concentration estimates from passive microwaves: Modelled and observed," *Int. J. Remote Sens.*, vol. 18, no. 5, pp. 1113–1136, Mar. 1997.
[35] D. J. Cavalieri, K. M. St. Germain, and C. T. Swift, "Reduction of weather effects in the calculation of sea-ice concentration with the DMSP SSM/I," *J. Glaciol.*, vol. 41, no. 139, pp. 455–464, 1995.
[36] S. Andersen, R. Tonboe, S. Kern, and H. Schyberg, "Improved retrieval of sea ice total concentration from spaceborne passive microwave observations using numerical weather prediction model fields: An intercomparison of nine algorithms," *Remote Sens. Environ.*, vol. 104, no. 4, pp. 374–392, Oct. 2006.
[37] E. Svendsen, C. Matzler, and T. C. Grenfell, "A model for retrieving total sea ice concentration from a spaceborne dual-polarized passive microwave instrument operating near 90 GHz," *Int. J. Remote Sens.*, vol. 8, no. 10, pp. 1479–1487, 1987.
[38] J. C. Comiso, D. J. Cavalieri, C. L. Parkinson, and P. Gloersen, "Passive microwave algorithms for sea ice concentration: A comparison of two techniques," *Remote Sens. Environ.*, vol. 60, no. 3, pp. 357–384, Jun. 1997.
[39] R. Tonboe and E. Nielsen, "Ocean and Sea Ice SAF Global Sea Ice Concentration Reprocessing Validation Product, Product OSI-409, EUMETSAT, Darmstadt, Germany, 2011, SAF/OSI/CDOP/met.no/TEC/RP/150, Tech. Rep. Version 1.3. [Online]. Available: http://www.osi-saf.org
[40] D. J. Cavalieri, T. Markus, and J. Comiso, "AMSRE/Aqua Daily L3 12.5 km brightness temperature, sea ice concentration, &snow depth polar grids Ver. 2. Digital media," NASA DAAC, Nat. Snow Ice Data Center, Boulder, CO, USA, 2003.
[41] D. J. Cavalieri, C. Parkinson, P. Gloersen, and H. J. Zwally, "Sea ice concentrations from Nimbus-7 SMMR and DMSP SSM/I-SSMIS passive microwave data," NASA DAAC, Nat. Snow Ice Data Center, Boulder, CO, USA, 1996.
[42] J. C. Comiso, "Bootstrap sea ice concentrations from Nimbus-7 SMMR and DMSP SSM/I-SSMIS. Digital media," Nat. Snow Ice Data Center, Boulder, CO, USA, 1999.
[43] Integrated Climate Data Center (ICDC), ASI Algorithm SSM/I-SSMIS Sea Ice Concentration Were Obtained for All Dates in Years 1992–2009, University of Hamburg, Hamburg, Germany, 2012. [Online]. Available: http://icdc.zmaw,de/
[44] J. C. Comiso and F. Nishio, "Trends in the sea ice cover using enhanced and compatible AMSR-E, SSM/I, and SMMR data," *Journal of Geophysical Research-Oceans*, vol. 113, no. C2, pp. C02S07-1–C02S07-22, Feb. 2008.
[45] D. K. Perovich *et al.*, "Field observations of the electromagnetic properties of first-year sea ice," *IEEE Trans. Geosci. Remote Sens.*, vol. 36, no. 5, pp. 1705–1715, Sep. 1998.
[46] T. C. Grenfell *et al.*, "Evolution of electromagnetic signatures of sea ice from initial formation to the establishment of thick first-year ice," *IEEE Trans. Geosci. Remote Sens.*, vol. 36, no. 5, pp. 1642–1654, Sep. 1998.
[47] B. J. Hwang, J. K. Ehn, D. G. Barber, R. Galley, and T. C. Grenfell, "Investigations of newly formed sea ice in the Cape Pathurst polynya: 2. Microwave emission," *J. Geophys. Res.*, vol. 112, no. C5, pp. C05003-1–C05003-14, May 2007.
[48] D. J. Cavalieri, "A microwave technique for mapping thin sea-ice," *J. Geophys. Res.—Oceans*, vol. 99, no. C6, pp. 12 561–12 572, Jun. 1994.
[49] A. P. Worby, K. M. Meiners, and S. F. Ackley, "Antarctic sea-ice zone research during the international polar year, 2007–2009," *Deep-Sea Res. II, Topical Stud. Oceanogr.*, vol. 58, no. 9/10, pp. 993–998, May 2011.

Alexander Beitsch received the Diploma degree in meteorology from the University of Hamburg, Hamburg, Germany, in 2010, where he has just received the Ph.D. degree with the Institute of Oceanography.

His research interests include satellite remote sensing of polar regions on the short time scale and polar climate variability on the long time scale.

Stefan Kern received the Diploma degree in meteorology from the University of Hannover, Hannover, Germany, in 1997 and the Ph.D. degree in physics from the University of Bremen, Bremen, Germany, in 2001.

Since 2001, he has been with the University of Hamburg, Hamburg, Germany, where he first worked with the Institute of Oceanography, and where he joined the Center of Excellence for Climate System Analysis and Prediction (CliSAP) in 2010. His main research interest is remote sensing of the marine cryosphere, algorithm development, evaluation, and uncertainty assessment, for an improved quantification of ocean–sea-ice–atmosphere interactions.

Lars Kaleschke received the Diploma in physics and the Dr. rer. nat. from the University of Bremen, Bremen, Germany, in 1998 and 2003, respectively.

He is a Professor with the Institute of Oceanography, University of Hamburg, Hamburg, Germany, and leads a research group for sea ice remote sensing. His research interests include remote sensing, the role of polar regions in the climate system, ice–ocean–atmosphere physicochemical interactions, and operational sea ice forecasting.